Chapter 1

Bunch length measurement

The length of a particle bunch is rather difficult to measure at lepton accelerators where this length is typically less than a millimeter, corresponding to bunch durations much shorter than what can be measured by fast detectors [1]. It is therefore necessary to convert the bunch length into another quantity that can be measured. Coherence is both a motivation and a tool to measure such length. Coherent collective effects such as coherent synchrotron radiation can significantly disrupt a beam. Their dependance on the beam current and not the beam charge means that to control them it is necessary to measure the bunch length instead of simply the bunch charge. As a counterpart, coherent radiation is one of the means of measuring a bunch length.

In plasma acceleration with external injection (such as FACET's E-200 [1], AWAKE [2] or ESCULAP [3]) this bunch length measurement is important to estimate which fraction of the bunch will fit in the acceleration buckets created in the plasma. As with the transverse measurements, at a plasma accelerator it is necessary to make the measurement in a single shot for it to be meaningful.

When the resolution is sufficient the bunch length measurement can become a bunch profile measurement as is the case with the methods based on coherent radiation methods.

I have worked on one of these techniques using Coherent Smith-Purcell Radiation for several years.

[1] Because in lepton accelerators the particles travel at the speed of light there is a direct correlation between bunch length and bunch duration. It results that abusingly the bunch length is often quoted with time units. A bunch duration of 1 ps corresponds to a bunch length of 0.3 mm

1.1 Bunch length and bunch profile measurement techniques

Several other techniques allow for bunch length measurements and I will first review them.

1.1.1 Techniques based on current transformers

Bunch charge can be measured using current transformers (CT). Depending on the application, there are several flavors of current transformers : AC-Current Transformers (ACCT), DC-Current Transformers (DCCT), Integrating Current Transformers (ICT), ... They all measure the current induced by the beam in a gap of the beam pipe to estimate the beam current. Depending on the signal amplification required the measurement device can be a simple wire connected to an ammeter or a coil with several windings connected to an ammeter or to more complicated electronics. The working principle and an example of current transformer are shown on figure 1.1.

When the time resolution of the current measuring device is good enough and the impedance low enough the current transformer can give information about the variation of the current with them and therefore the bunch length, however this is true only for beams that are at least several centimeters long (nanosecond duration).

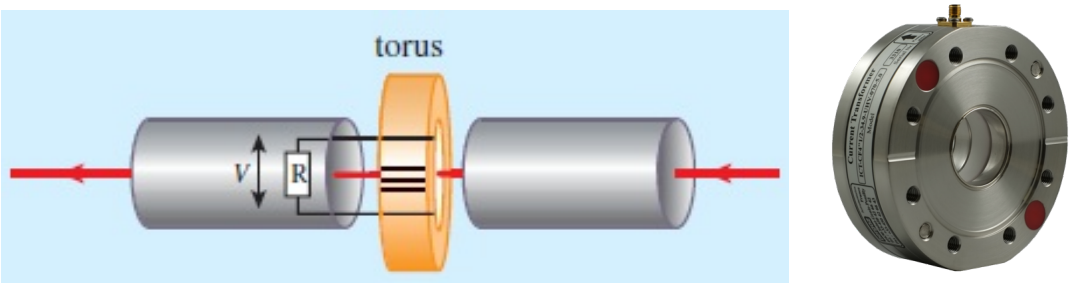

Figure 1.1: (Left) Principle of a current transformer used for beam charge measurement : when the particle beam passes through a torus it induces a current proportional to the beam charge in the torus coil windings, allowing for beam charge measurement. (Right) Example of current transformer as sold by a well-known manufacturer [4].

1.1.2 Techniques based on longitudinal to transverse exchange

For beam with a length in the millimeter range (or below) it is more difficult to measure their length or their profile in the longitudinal direction (that is the direction of propagation) than their transverse properties. Exchanging the longitudinal direction with one of the transverse directions can therefore make this measurement easier.

A **Streak Camera** is a device available commercially that can achieve this fate : in a streak a photon beam hits a photocathode and is converted by photoemission in a low energy (keV) electron beam. This electron beam passes between two electrodes to which are applied a high frequency high voltage electric field that will streak the electron beam transversely, the electron deflection being proportional to their arrival time. After the electrodes the electron beam hit a luminescent screen where the transverse profile of the electrons after streaking can be observed. Thus it is possible to obtain the longitudinal profile of the photon beam (convoluted with one of its transverse profile). Commercial streak camera can reach a resolution of about 1 ps on photon beams.

A **Streak Camera combined with a radiation emitting screen**, such as a sapphire screen emitting Cerenkov radiation can be used to image the longitudinal profile of an electron beam with MeV energy or higher. Such method was tested for example at the CANDELA photo injector at LAL [5]. However this method is limited by the spread in the longitudinal profile induced by the screen itself and by the photon beam transport (usually to the outside of the accelerator) and therefore it is not available to measure sub-picoseconds beams.

Streak camera are often used in rings to measure the bunch length using the synchrotron radiation emitted[6, 7].

This can be mitigated by deflecting directly the high energy electrons using a **deflecting RF cavity**. This requires the electric field to be high enough to deflect high energy electrons and to have a high enough frequency to streak significantly the beam. The state of the art in this field has been demonstrated at SLAC recently on both LCLS and FACET accelerators [8], reaching resolutions of 10 fs at 14 GeV and SI70fs at 20 GeV. However the cost of such device, including the associated RF power source is more than a million euros.

A cheaper solution to streak the electrons is to use the so-called **3-phases method** [9, 10] in which one of the accelerating section of the accelerator is dephased to provide a longitudinal streaking effect that can be measured as a variation in the beam energy dispersion. This method has the advantage of being much cheaper but is limited in its resolution by the power of the accelerating cavity and the resolution of the dispersion measurement setup. A resolution of a few picoseconds has been demonstrated experimentally.

1.1.3 Measures based on radiation emitted by the beam

Instead of manipulating the beam to measure it, it is possible to measure the radiation it emits and use it to get information on its longitudinal profile. This is what is done with the streak camera based measurements described above but other methods rely on this technique.

In the **electro-optic sampling** method a birefringent crystal is brought close from the

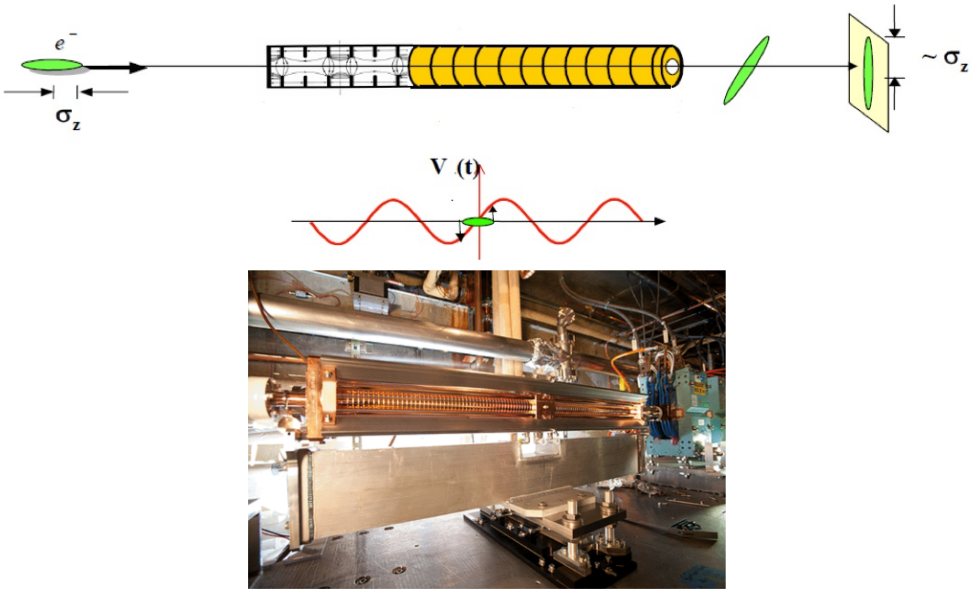

Figure 1.2: Left: The principle of the Transverse deflecting cavity used at SLAC to measure bunches longitudinal profiles (Image taken from https://portal.slac.stanford.edu/sites/ard_public/facet/facilities/Pages/TCAV.aspx). Right: A photo of the FACET transverse deflecting cavity (image taken from [8]).

electron beam and a chirped ultrafast laser pulse[2] is shone on it. The electromagnetic field of the electron beam will induce a change in the refraction index of the crystal in at least one of the polarisation plane. As the laser pulse is chirped a diffraction grating can then be used to measure its longitudinal profile projected on a screen. Thus by comparing the longitudinal profile of the two polarisation components it is possible to deduce the changes that occurred in the crystal as fonction of time and therefore the bunch longitudinal profile. This is a well known technique in optics (for example to measure and profile THz pulses) that has been applied to accelerators by several groups (including, for example, [11, 12, 13]). This technique is illustrated on figure 1.3.

The electromagnetic spectrum emitted by the electron bunch is modulated by the bunch length: when a photon is emitted in an electron bunch, if the wavelength of that photon is larger than the separation between two photons, then the two photons will contribute and the emission probability is increased. When N photons contribute the probability increases as $N(N-1)$.

It is possible to define the "form factor" ($\mathcal{F}$) of the radiation emitted by an electron bunch as:

[2]This means that the photons of the laser pulse have a correlation between wavelength and longitudinal position. This is a common techniques with lasers and can be done, for example, by using a set of diffraction gratings.

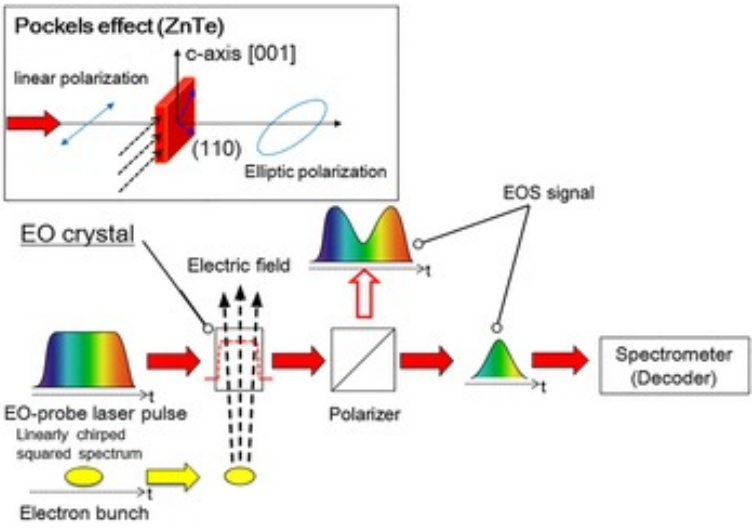

Figure 1.3: Principle of bunch length measurements using electro-optic sampling (taken from [13]

$$\mathcal{F}(\nu) = \left|\int_{-\infty}^{+\infty} S(x)\exp\left(i\frac{2\pi\nu}{c}x\right)dx\right| \times \left|\int_{-\infty}^{+\infty} S(y)\exp\left(i\frac{2\pi\nu}{c}y\right)dy\right| \times \left|\int_{-\infty}^{+\infty} S(z)\exp\left(i\frac{2\pi\nu}{c}z\right)dz\right| \tag{1.1}$$

where ν is the photons' frequency, $S(x)$, $S(y)$ and $S(z)$ are the profile distribution along x, y and z respectively. And the total radiation intensity I_{tot} emitted for a given radiative phenomena at a given frequency will be:

$$I_{tot}(\nu) = I_1(\nu)\left(N + N(N-1)\mathcal{F}(\nu)\right) \tag{1.2}$$

where I_1 is the single electron yield for the phenomena and N the number of electrons. This radiation can be used in several different manners to measure the bunch length and its longitudinal profile.

Coherent Transition Radiation (CTR) is emitted when a bunch of charged particles passes through a thin foil. Several groups [14, 15, 16] have studied how to measure the spectrum of the CTR emitted and used it to reconstruct bunch length. The SLAC group [14] uses a KRS-5 prism to disperse the infrared radiation collected and focus it on a detector. The Frascati group [15] uses a Martin-Puplett interferometer to study the THz radiation produced by their CTR screens. These setups are shown on figure 1.4. It should be noted that the methods used by these two groups require a scan of the dispersive element or of the interferometer to measure the radiation spectrum. To overcome this difficulty the DESY group [16] uses several dispersive gratings with several detectors to perform this measurement (see figure 1.5).

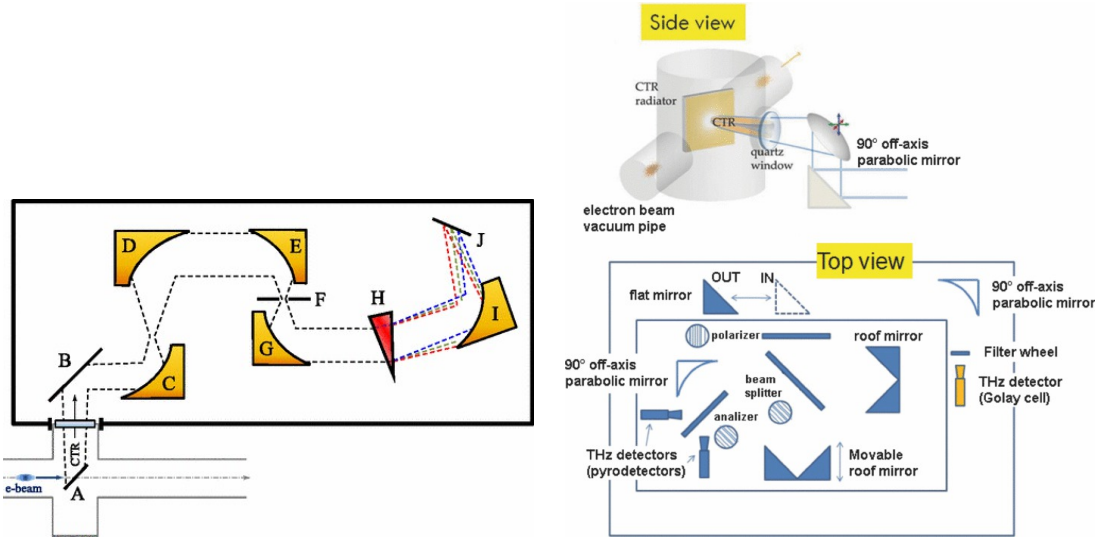

Figure 1.4: Principle of Coherent Transition Radiation measurements at SLAC on LCLS and FACET (left; taken from [14]) and at SPARC (right taken from [15]).

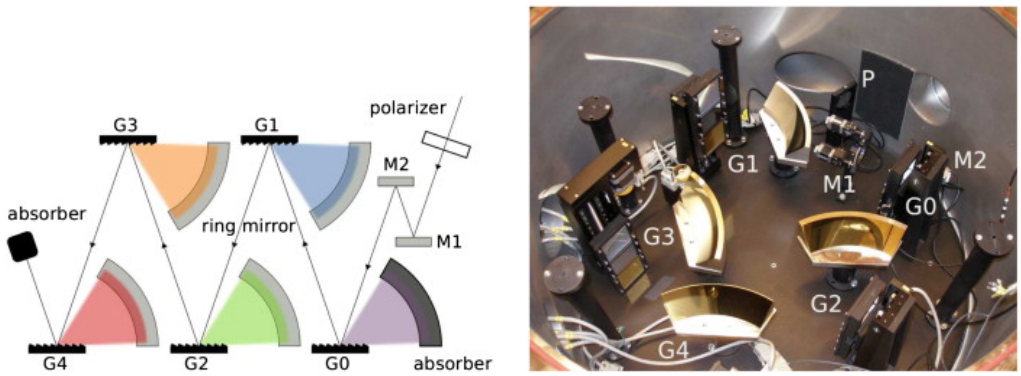

Figure 1.5: Principle XX of the Coherent Transition Radiation single shot setup at DESY (schematic and picture).

The SLAC group has published their ability to reconstruct 3 fs to 60 fs-long bunches.

Another way to measure the radiation emitted by the bunch is to measure the **Coherent Smith-Purcell Radiation (CSPR)** it emits. CSPR is emitted when a metallic diffraction grating is brought close from the beam. I have worked extensively on CSPR for several years and it is described details in section 1.2.

1.1.4 Comparison of longitudinal bunch measurement techniques

The different longitudinal bunch measurement techniques are summarized in tables 1.1 and 1.2.

From theses tables it appears that there is a wide range of cost and complexity among longitudinal bunch length measurements. The use of RF deflecting cavities is both complex and expensive (the price been dependent on the beam energy and the RF band chosen for the measurement) but it is used at several accelerators as a reference to measure the bunch length [3]. This has triggered research to find cheaper techniques. Electro-optic sampling is a technique that was already available from the optics community, however it is complex as it requires an ultrafast laser that is hardly compatible with an accelerator enclosure and therefore requires to transport the ultrashort laser pulses inside the accelerator enclosure. CTR has the advantage of being even cheaper and less complicated to setup and several groups have investigated it and solved differently the problem of spectrum measurement. CSPR is a less known phenomena and therefore it has been investigated by fewer groups but renewed interest appeared because of its single shot and non-destructive capability.

The interest for Energy Recovery Linac (ERL) may also increase the need for non destructive single shot longitudinal diagnostics: current ERLs have shown that correct operations require a very good understanding of the bunch longitudinal phase space at different locations along the ERL. The availability of a non destructive fast diagnostics would therefore be an advantage for such machine and in particular for the machine that is planned to be built in Orsay.

[3] A comparison of Electro-optic sampling, streak cameras and RF deflecting cavities as longitudinal bunch profile diagnostic for FACET has been published in [17].

Name	Main technology	Best resolution	Cost	Availability status
Current transformer	Coil	Limited by electronics $\mathcal{O}$ 100 ps	$\mathcal{O}$ 10k€	Commercially available Commonly used
Streak camera with radiator	Photocathode, High Voltage	Limited by high voltage frequency $\mathcal{O}$ ps	$\mathcal{O}$ 300k€	Camera commercially available Setup: R&D
RF deflector	High power RF + cavity C-band or X-band RF	$\mathcal{O}$ 10 fs	$\mathcal{O}$ 500k€- 2M€ (energy dependent)	R&D product distributed by one manufacturer
3 phases	RF cavities	$\mathcal{O}$ ps	Use linac infrastructure	Commonly used
Electro-optic sampling	Laser Birefringent crystals	$\mathcal{O}$ 50 fs (better res. in optics)	Laser: $\mathcal{O}$ 200k€ Other: $\mathcal{O}$ 50k€	Commonly used in optics
Coherent Transition Radiation	Optics THz filtering	$\mathcal{O}$ 10 fs	$\mathcal{O}$ 50k€	In use at several facilities
Coherent Smith-Purcell Radiation	Diff. gratings THz filtering	$\mathcal{O}$ 50 fs	$\mathcal{O}$ 50k€	R&D

Table 1.1: Comparaison of the properties of the different techniques of longitudinal bunch length and profile measurement

Name	Single shot capability	Beam destruction
Current transformer	Yes	No
Streak camera with radiator	Yes	Radiator dependent Synchrotron radiation: No; Screen: Yes
RF deflector	Partially The phase of the measurement must be checked	Yes
3 phases	No	Yes (beam off-energy)
Electro-optic sampling	Yes	No
Coherent Transition Radiation	Interferometer: No Multpl. Gratings: Yes	Yes
Coherent Smith-Purcell Radiation	Yes	No

Table 1.2: Comparaison of the capabilities of the different techniques of longitudinal bunch length and profile measurement

1.2 Smith-Purcell Radiation

1.2.1 First observation of Smith-Purcell Radiation

The first observation of what is now called Smith-Purcell Radiation dates back to 1953 when Smith and Purcell reported the observation of visible light from localized surface charges moving across a grating [18]. Their observation was made using 300 keV electrons in a continuous beam. An image of this observation is shown on figure 1.6.

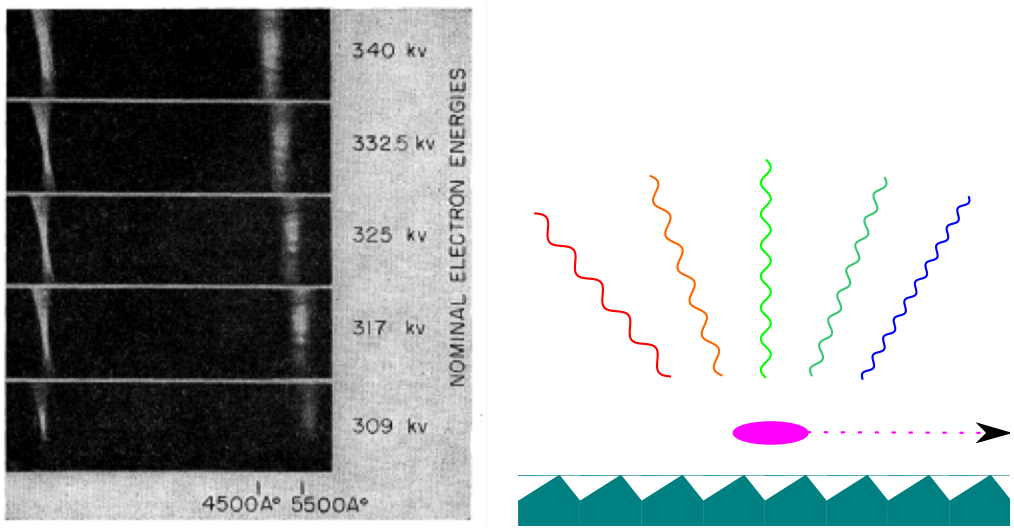

Figure 1.6: Left: Image taken from [18] showing the observation of radiation by Smith and Purcell in 1953. Right: Schematic of Smith-Purcell radiation.

The first observation of Smith-Purcell radiation from relativistic electrons was reported only much later in 1992 [19] and the first observation of Coherent Smith-Purcell Radiation [20] came in 1995.

XXX coherent / relativistic images

XXX Van den berg P. M. van den Berg, J. Opt. Soc. Am. 63, 1588 1973!.

1.2.2 Interpretation of Smith-Purcell Radiation

The phenomena was further studied and several interpretations were proposed:

- According to Ishiguro and Tako's interpretation [21], Smith-Purcell radiation comes from dipole radiation: when an electron beam passes above a grating it induces a current in the grating; the oscillations of this current in the teeth of the grating will create dipole radiation that is emitted. This will later be referred to as the "surface current" interpretation. This interpretation is shown on figure 1.7 (left).

- Toraldo di Francia proposed a different interpretation [22]: according to him a charged particle in straight uniform motion generates a field that can be expanded into a set of evanescent waves. It is the diffraction of these waves on a diffraction grating that creates the Smith-Purcell radiation. This will later be referred to as the "radiation diffraction" interpretation. This interpretation is shown on figure 1.7 (right).

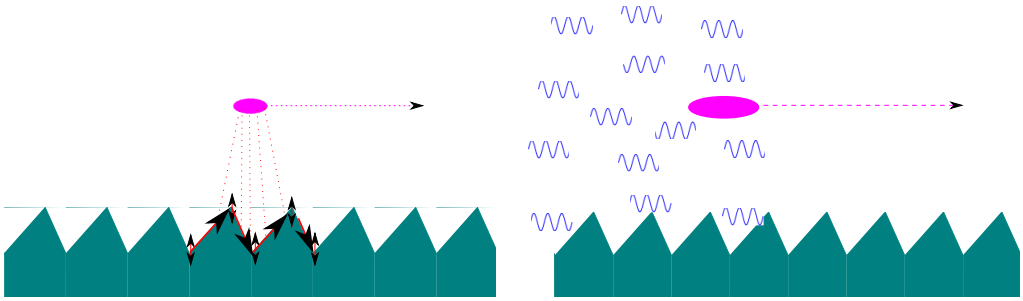

Figure 1.7: The two interpretation of Smith-Purcell radiation: The surface current interpretation as in [21] (left) and the radiation diffraction interpretation as in [22] (right).

Although these interpretations are different, the underlying physics is the same and the interpretations should yield to comparable predictions. A comparison of several Smith-Purcell radiation models has been published in [23] and based on that paper I worked with a student to perform such comparison for parameters relevants to the experiments we were conducting [24]. Our conclusion was that within an order of magnitude all models have to comparable single electron yield as shown on figure 1.8.

1.2.3 Application of Smith-Purcell Radiation

Smith-Purcell radiation and later CSPR have been seen by many scholars as a potential source of high power infrared radiation, leading for example to a patent to that purpose [27]. As early as 1979, Smith-Purcell radiation has also been seen by some scholars as a promising tool to seed Free Electron Lasers [28, 29, 30, 31, 32] and has been patented [33].

The use of CSPR as a bunch longitudinal profile diagnostic was proposed soon after the first observation of CSPR and it was even patented [34] (for the US only) at that time. More detailed work was published by a different team in 2002 [35, 36] and several key steps were done in the following years [37, 38], including in teams in which I was participating [39, 40, 41, 42].

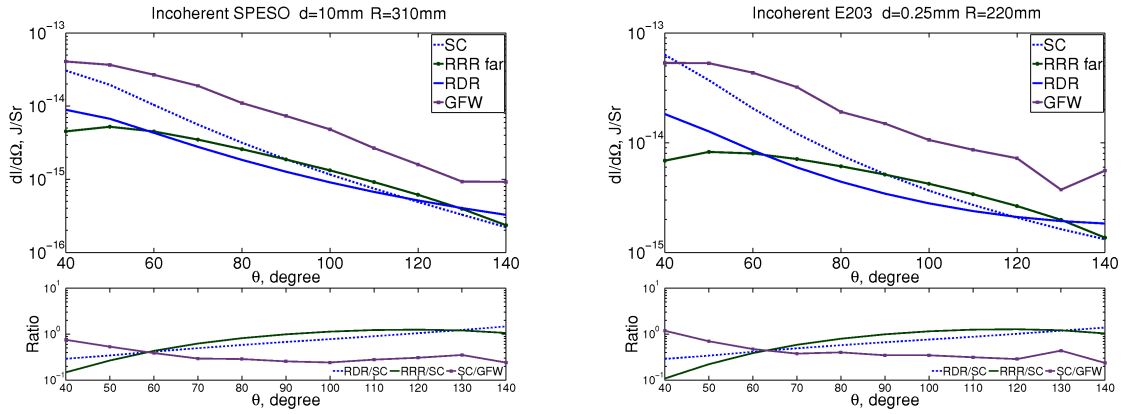

Figure 1.8: Comparison of the single electron yield of different Smith-Purcell Radiation models (as published in [24]): the solid blue line corresponds to the Resonant Diffraction Radiation (RDR) model [23], the green line to the Resonant Reflection Radiation (RRR) model [25], the purple line with square marker label GFW to the Surface Current model as described in [26] and the blue dashed line also to the Surface Current (SC) model described in [26] but with the grating coupling efficiency expression taken from [23]. See [24] for details.

1.2.4 Theoretical aspects of Smith-Purcell Radiation

The theory of Smith-Purcell radiation has been developed in several publications. The most relevant of them, based on the surface current model, being [26, 43]. The discussion below is based on these articles.

A diffraction grating will reflect light in different directions by interferences between the rays reflected by each surface. As shown on figure 1.10, reflections corresponding to the simple Snell-Descartes law are called "Order 0". Higher order correspond to interferences between all the teeth (order 1) or part of the teeth.

The coordinate system used in this chapter is shown on figure 1.9.

The relation between the polar angle of observation θ (in the plane perpendicular to the grating surface and passing by the beam), the grating pitch l and the wavelength λ of the emitted radiation is given by

$$\lambda = \frac{l}{n}\left(\frac{1}{\beta} - \cos\theta\right) \tag{1.3}$$

where n is the radiation order and $\beta = \frac{v}{c}$ is the ratio between the particle speed v and the speed of light c. In lepton accelerator it is often very close to 1. This relation is purely a consequence of the fact that waves emitted by a grating will interfere and in each direction constructive interferences correspond to specific wavelengths.

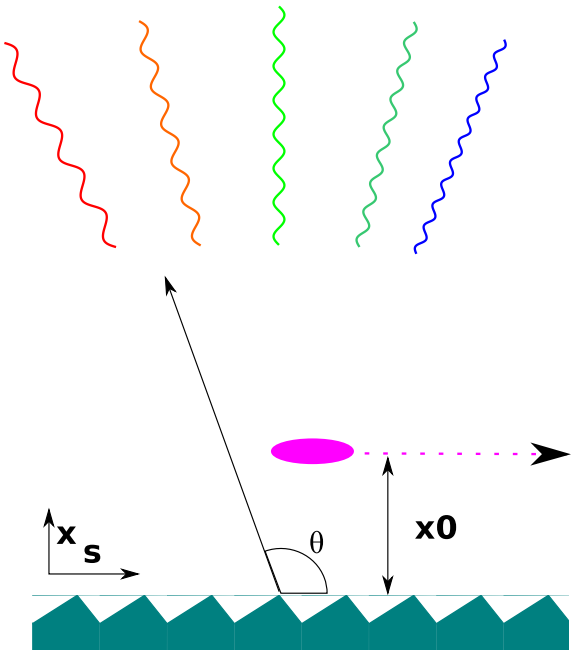

Figure 1.9: Coordinates system used in this chapter. The direction z comes out of the figure plane as is the azimuthal angle ϕ.

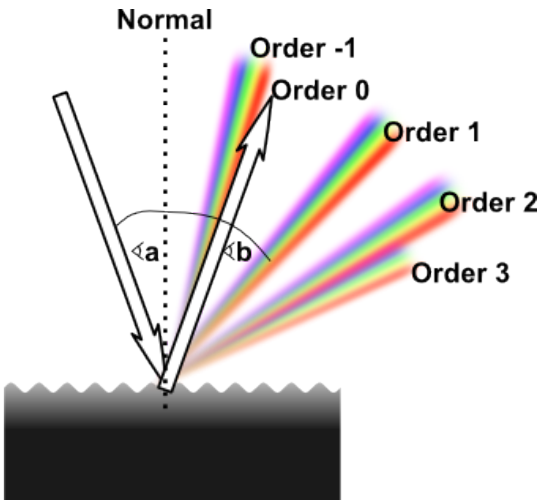

Figure 1.10: The different orders of a grating: order 0 corresponds to a simple reflection, the other orders corresponds to interferences of the wavelengths reflections. Image taken from [44].

The intensity of radiation emitted by a single electron (single electron yield), per unit solid angle (Ω) is given by

$$\frac{dI_1}{d\Omega} = \frac{L}{l^2}\frac{2\pi e^2 n^2 \beta^2}{(1-\beta\cos\theta)^3} R^2 \exp\frac{-2x_0}{\lambda_e} \tag{1.4}$$

where e is the electron charge, L the grating length, x_0 is the beam grating separation, λ_e is the evanescent wavelength of the virtual radiation emitted by the beam and R^2 is a factor reflecting the coupling of the beam with the grating.

The evanescent wavelength is given by

$$\lambda_e = \lambda\frac{\beta\gamma}{2\pi\sqrt{1+(\beta\gamma\sin\theta\sin\phi)?2}} \tag{1.5}$$

where γ is the Lorentz factor, ϕ is the azimuthal angle (the ascension above or below the plane perpendicular to the grating surface and passing by the beam).

An example of values of single electron yield taken from [45] is shown on figure 1.11.

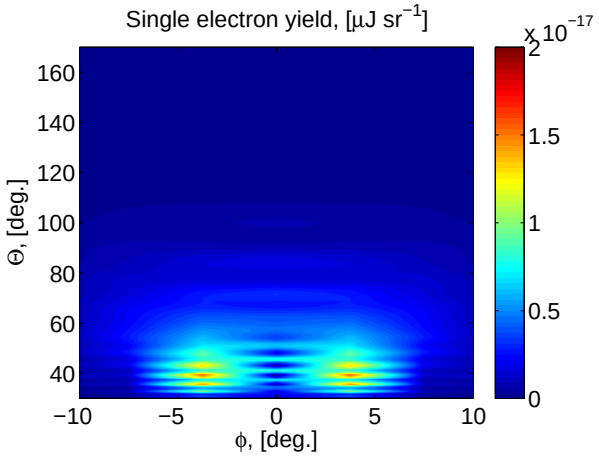

Figure 1.11: Single electron yield of Smith-Purcell radiation for a 40×180 mm^2 grating with a 8 mm pitch and a30^o blaze angle. Image taken from [45].

As discussed above, equation 1.2 applies to Smith-Purcell Radiation and the total radiation intensity emitted from a charged particle bunch of multiplicity N is given by:

$$\frac{dI}{d\Omega} = \frac{dI_1}{d\Omega}\left[N + N(N-1)\mathcal{F}(\omega)\right] \tag{1.6}$$

where $\mathcal{F}(\omega)$ is the form factor introduced in equation 1.1.

On figure 1.12 one can see a comparison of different profiles with the same FWHM (5 ps) but with different shapes and how this changes the expected CSPR signal.

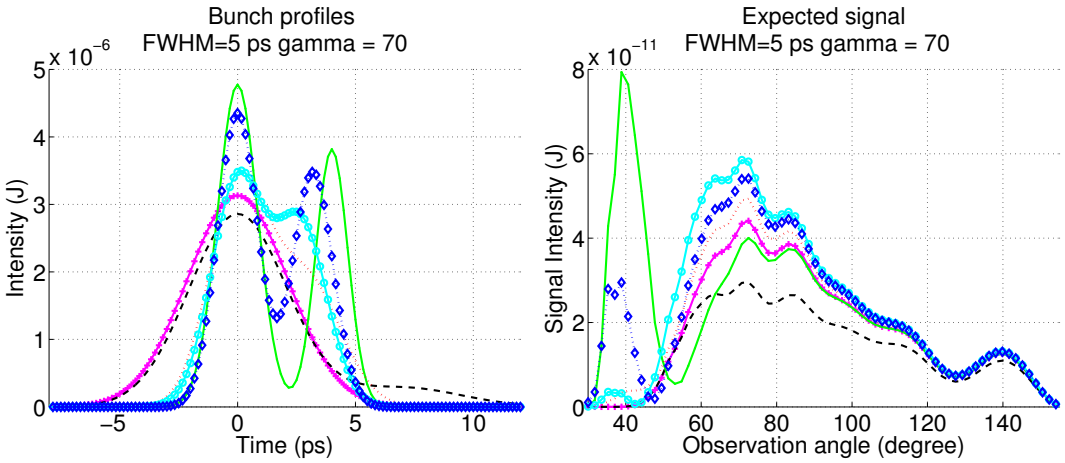

Figure 1.12: Comparison of several bunch profiles with the same FWHM (5 ps) but with different shapes (left) and predicted CSPR signal for each of these profiles (right). The capability to distinguish internal features of the beam and in particular substructures appears clearly. The parameters used for these simulations are based on the experiment done at CLIO (see section 1.3.3).

One important difference between CSPR and other radiative methods is that the choice of the grating will change the radiation intensity observed at different frequencies. On figure 1.13 one can see the radiation intensities observed for the same bunch profile but with different gratings pitches.

Improving the beam-coupling calculation

The factor R^2 is rather complicated to estimate. It has been discussed in details in [46] and an approximate solution has been given for high energy beams in the case of echelette gratings.

The equation 1.3 is very similar the the standard grating equation in the Littrow condition (with the same definition of variables as above) [47]:

$$\lambda = \frac{2l \sin\theta}{n} \tag{1.7}$$

This has led me to study with two students [48, **?**] whether it would be possible to benefit from the advanced work done in the field of grating theory [49] to estimate R^2. We produced some predictions but these are rather close to what has been obtained with simulation codes based on [46] and therefore we have not yet been able to distinguish the two approaches. This may become possible at the experiment described in 1.3.3.

It should be noted that with the advent of fast and powerful Particle-in-cell electromagnetic simulation softwares, it becomes possible to simulate the electromagnetic effects

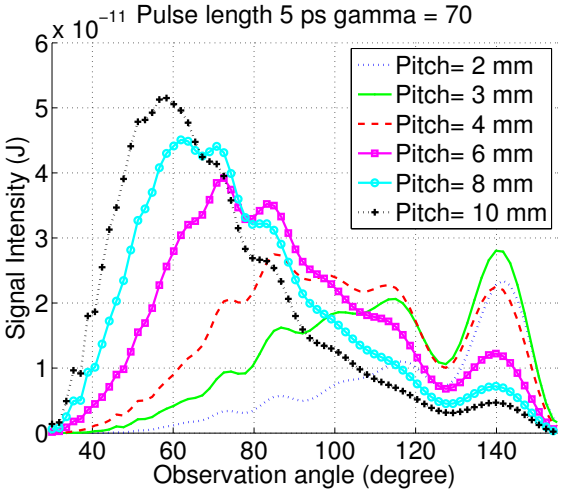

Figure 1.13: Radiation profiles observed for the same pulse but for different grating pitches. The parameters used for these simulations are based on the experiment done at CLIO (see section 1.3.3).

that a charged particles beam induces near a grating without relying on the models described above. This is what has been attempted in [50].

1.2.5 Profile recovery

As we can see in equation 1.6, there is a mathematical relation between the form factor and the CSPR intensity at each wavelength. Using relation 1.3 we see that this means that the signal intensity measured at different angles depends on the form factor and therefore encodes the bunch length. Calculating the form factor from the measured signal is therefore rather straightforward.

We have also seen in equation 1.1 that the form factor is strongly related to the bunch longitudinal profile. However the inverse operation is not so easy: some information is lost due to the absolute values in equation 1.1. The knowledge of the form factor alone requires more complicated mathematics to recover the profile.

The Fourier transform of a physical function satisfies the Cauchy-Riemann equations therefore a given real function (the measured form factor) can only be matched to a very limited number of imaginary functions and usually by adding extra conditions there will be only one remaining acceptable imaginary (phase) function. This phase function can be found using a Hilbert transform or the Kramers Kronig (KK) relations.

To recover the phase of a form factor, it must first be written in the following form:

$$log(\mathcal{F}(\omega)) = log(\rho(\omega)) + i\Theta(\omega) \tag{1.8}$$

where $\rho(\omega))$ is the amplitude and $\Theta(\omega)$ the phase associated to this Form factor. $\rho(\omega))$ is thus the result of the measurement and $\Theta(\omega)$ the information that needs to be recovered.

The Hilbert transform gives then the relation

$$\Theta(\omega_0) = -\frac{1}{\pi} P \int_{-\infty}^{+\infty} \frac{ln(\rho(\omega))}{\omega_0 - \omega} d\omega. \tag{1.9}$$

and the Kramers Kronig relation gives:

$$\Theta(\omega_0) = \frac{2\omega_0}{\pi} P \int_{0}^{+\infty} \frac{ln(\rho(\omega))}{\omega_0^2 - \omega^2} d\omega \tag{1.10}$$

In most cases the value given by these two methods will be very close.

Before I started working on CSPR an algorithm based on KK was already available [51] for all coherent radiation phenomena. However its implementation for CSPR was sometimes leading to non-sensical results. With a student (Vitalii Khodnevych), we implemented and studied a new phase recovery algorithm based on the Hilbert transform [52]. We extended this work by doing a large number of simulations to also study the precision of this algorithm, how to optimise the position and number of detectors and how noise can affect the quality of the measurement [53]. The main results of this paper are presented below.

To study how profiles shapes match each other we defined a variable by analogy to the standard Full-Width at Half-Maximum (FWHM), this variable called Full-Width at X of the Maximum (FWXM) allows to study the width of a pulse at a certain fraction X of the maximum. The FW0.5M is similar to the usual FWHM. To compare the shape of a reconstructed profile (deco) and its orignal (orig) we define the variable Δ_{FWXM} as follow:

$$\Delta_{FWXM} = \left| \frac{FWXM_{\text{orig}} - FWXM_{\text{reco}}}{FWXM_{\text{orig}}} \right| \tag{1.11}$$

Figure 1.14 for example shows example of simulated profiles correctly reconstructed but also profiles poorly reconstructed. Figure 1.15 studies the impact of the number of detectors of the quality of the reconstruction, showing that there is an optimum at about 3×11 detectors (3 sets of 11 detectors covering different frequency ranges) and figure 1.16 shows that positioning them at constant angle is better than positioning them linearly or logarithmically (in frequency), examples of possible detectors positioning are shown on figure 1.17. Finally we also studied the effect of noise on the measured signal on the quality of the reconstruction 1.18.

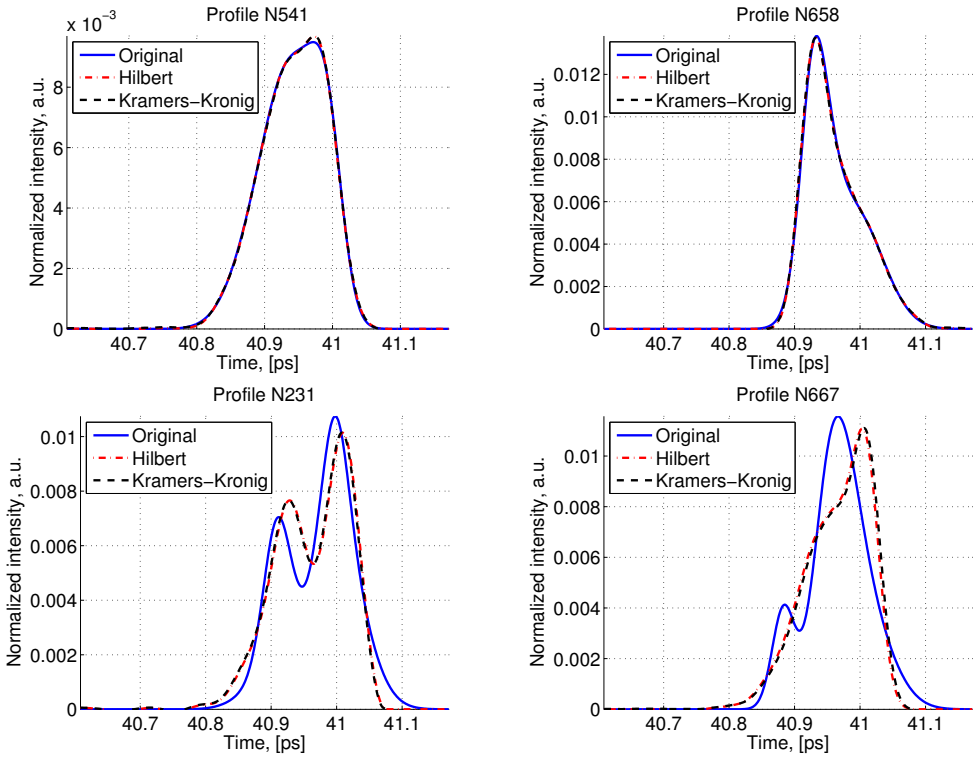

Figure 1.14: Example of profiles correctly reconstructed (upper row) and poorly reconstructed (lower row) as presented in [53]. The original profile is in blue and the profiles reconstructed with the Hilbert transform and the full Kramers-Kronig procedures are in red and black respectively.

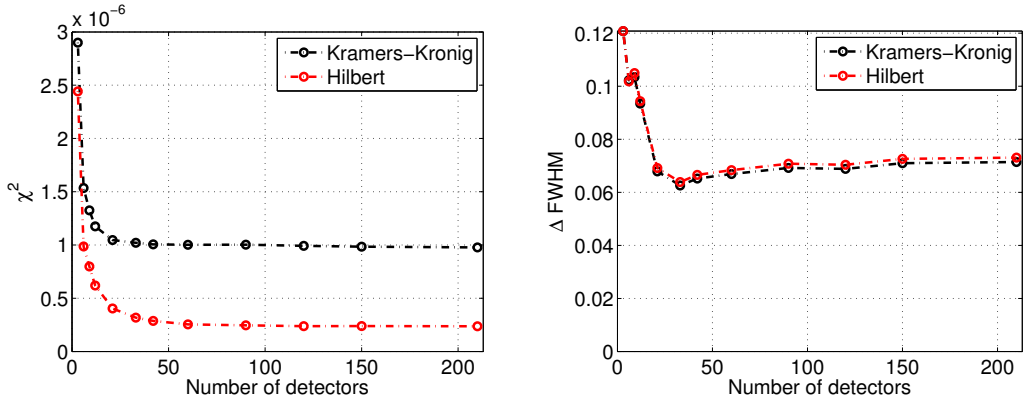

Figure 1.15: Effect of the sampling frequencies (number of detectors) on the χ^2 (left) and Δ_{FWHM} (right) when comparing original an reconstructed profiles, as presented in [53].

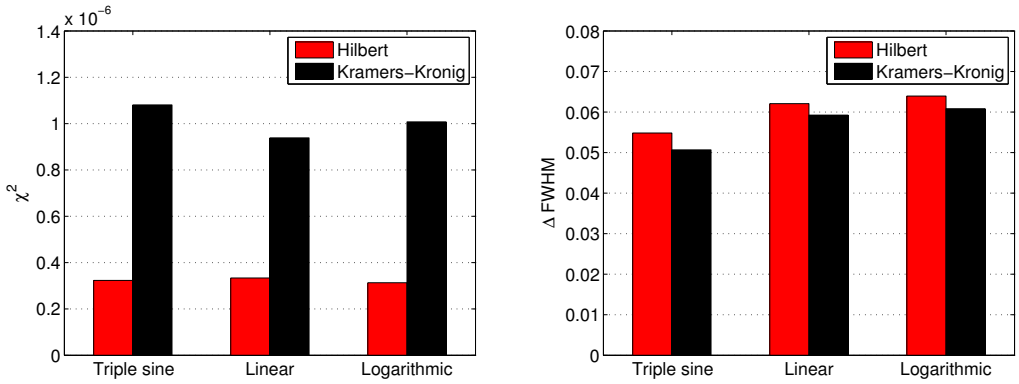

Figure 1.16: Comparison of different samplings methods using the χ^2 criterion (left) and Δ_{FWHM} (right), as presented in [53].

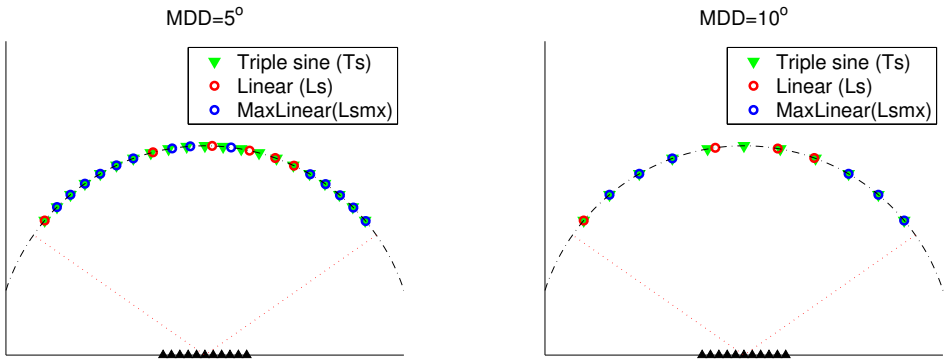

Figure 1.17: Examples of detector positions for different types of sampling for a minimal detector distance of 5^o (left) and 10^o (right), as presented in [53] .

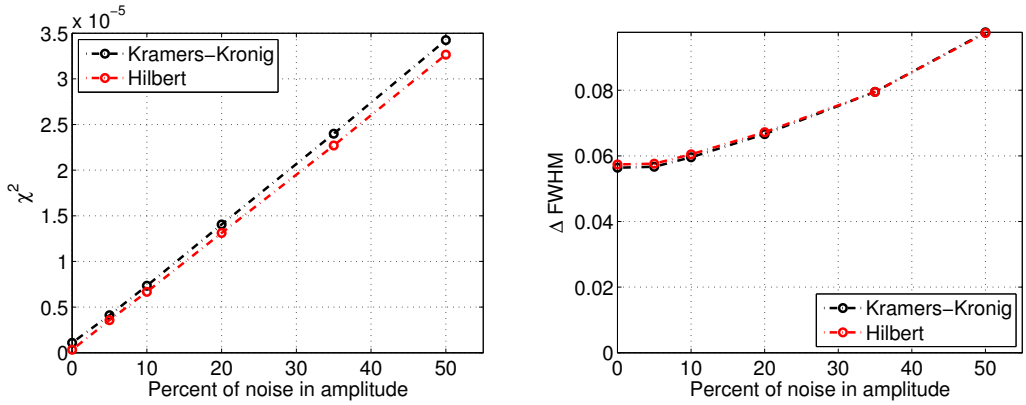

Figure 1.18: Mean χ^2 and Δ_{FWXM} as function of the noise amplitude, as presented in [53]. The interpretation of this figure is that with a 50% noise on our signal we introduce an error on the profile FWHM of about 10%.

Near field, far field and pre-wave effects

As the Smith-Purcell radiation is formed by a grating, there is a formation length and the number of teeth of the grating, the distance between the grating and the detector have to be taken into account. The line width of the radiation is given by the formula:

$$\frac{\delta\lambda}{\lambda} = \frac{l}{nL} \tag{1.12}$$

The effect of the grating-detector distance has been discussed in details in [42].

With a student I also studied the predictions for the pre-wave effect [54] and this work shows that corrections might have to be applied, especially at very high energy. However owing to the non observation of this effect in [55] as discussed in section 1.4, experimental verification of the effect of pre-wave interferences and accurate calculation are needed. Experimental attempts will be discussed in section 1.3.2.

1.3 Experimental study of Coherent Smith-Purcell radiation

When I joined the effort at the University of Oxford on CSPR our main goal was to demonstrate that CSPR could be used as a longitudinal profile diagnostic in the sub-picosecond regime. The work would lead to the E-203 collaboration that took data at SLAC. Later, after I moved to Orsay, I decided to extend this effort to better understand the properties of CSPR using a test setup installed at SOLEIL and called SPESO and to also study how to make CSPR a tool available in accelerators control room, by making experiments on the CLIO accelerator.

1.3.1 Smith-Purcell radiation measurement at FACET: E-203

FACET (Facility for Advanced Accelerator Experimental Tests) was a 20 GeV electron accelerator installed on the SLAC campus in Stanford, California [56]. It had the advantage of being the only test facility offering easy access to sub-picosecond bunches.

In 2010 we proposed to re-use the hardware from a previous experiment [38] to use it at FACET to measure sub-picosecond bunches. This led to the formation of the E-203 collaboration.

The experiment has been described in details in [40]. It consists of a carousel on which 3 different gratings and a blank (a flat grating without teeth are mounted). This carousel can be moved inside the accelerator vacuum to bring the grating close from the beam. Opposite to the carousel there are 11 silicon windows located every 10° in θ from 40° to 140°. Outside the movable windows waveguide array plates (WAP) filters are used to filter only the radiation at the wavelength expected from the selected grating. After the filters Winston cones concentrate the radiation within their acceptance onto pyroelectric detectors. Several pictures of the E-203 experiment are shown on figure 1.19 and the optical elements are shown on figure 1.20.

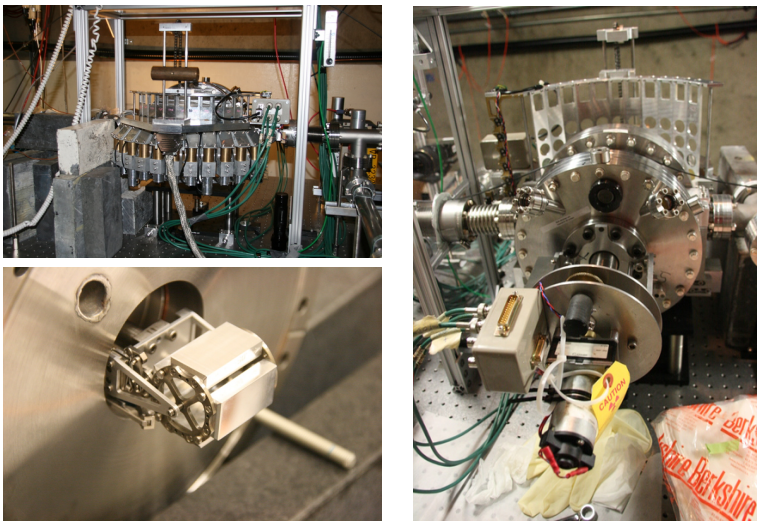

Figure 1.19: The E-203 experiment (during pre-installation tests) seen from the detectors side (top left), from the motors side (right) and the grating's carousel (bottom left). Images taken from [41].

The experiment was successful in measuring sub-picosecond bunches [40, 42, 41]. and examples of the profiles measured are shown on figure 1.21.

Background rejection is an important problem for radiative measurements. Because CSPR uses the dispersion induced by the grating it is less sensitive than other methods but still not immune. One method to measure the background is to expose a "blank"

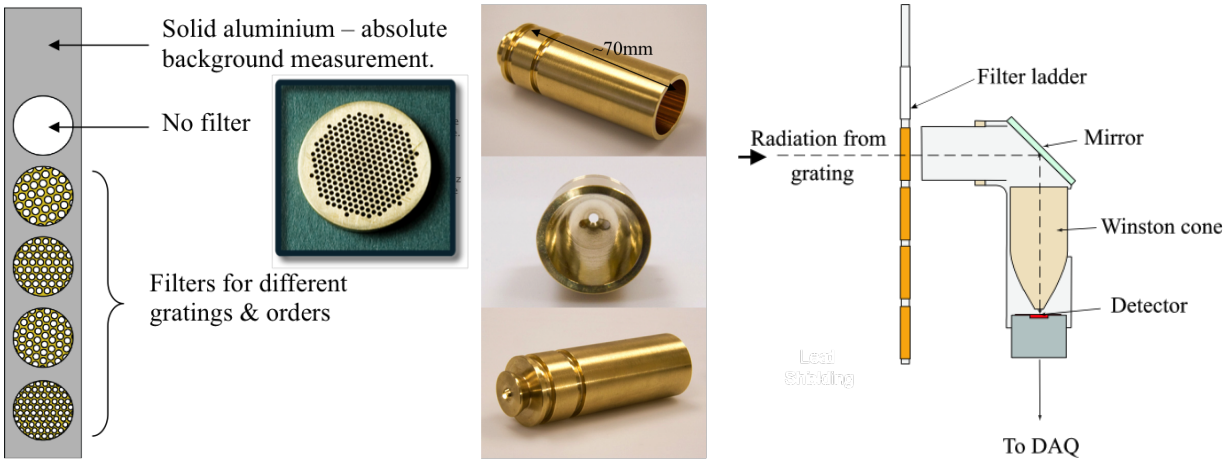

Figure 1.20: The optical parts of the E-203 experiment: (from left to right) the filters, the optical concentrators (winston cones) and the optical assembly (image taken from [42]).

grating, that is a grating without teeth, to the beam and measure the signal produced. This signal is then considered to be the background.

Another solution could be to measure the two polarisation components of the signal: CSPR is known to be polarized whereas most backgrounds aren't. We verified this with the E-203 apparatus [42] (see figure 1.22). and I worked further on that topic with a student who had taken part in the experiment [48].

Additional measurements of the polarization and the azimuthal distribution of CSPR have been done by the E-203 experiment and are being analyzed.

1.3.2 Smith-Purcell radiation measurement at SOLEIL: SPESO

Many questions about Smith-Purcell arose when we formed the E-203 collaboration and FACET being far from Europe, it was not the best suited place to make detailed comparison between theory and experimental results.

With colleagues from Synchrotron SOLEIL I therefore started another experiment called SPESO (Smith-Purcell Experiment at SOLEIL). SPESO is installed at the end the Helios, the SOLEIL linac. For simplicity reasons SPESO uses a fixed grating on a movable arm. Opposite to this window is a z-cut quartz window (transparent at the wavelengths at which the radiation is expected). In front of that window a set of 3 translation stages and 4 rotation stages allow to move detectors in 3D and mesure the intensity of Smith-Purcell radiation at different locations. The layout of the experiment is shown on figure 1.23 and a photo is shown on figure 1.24. The experiment has been described in details at [57].

The first SPESO signal was difficult to obtain because the pulse length had been un-

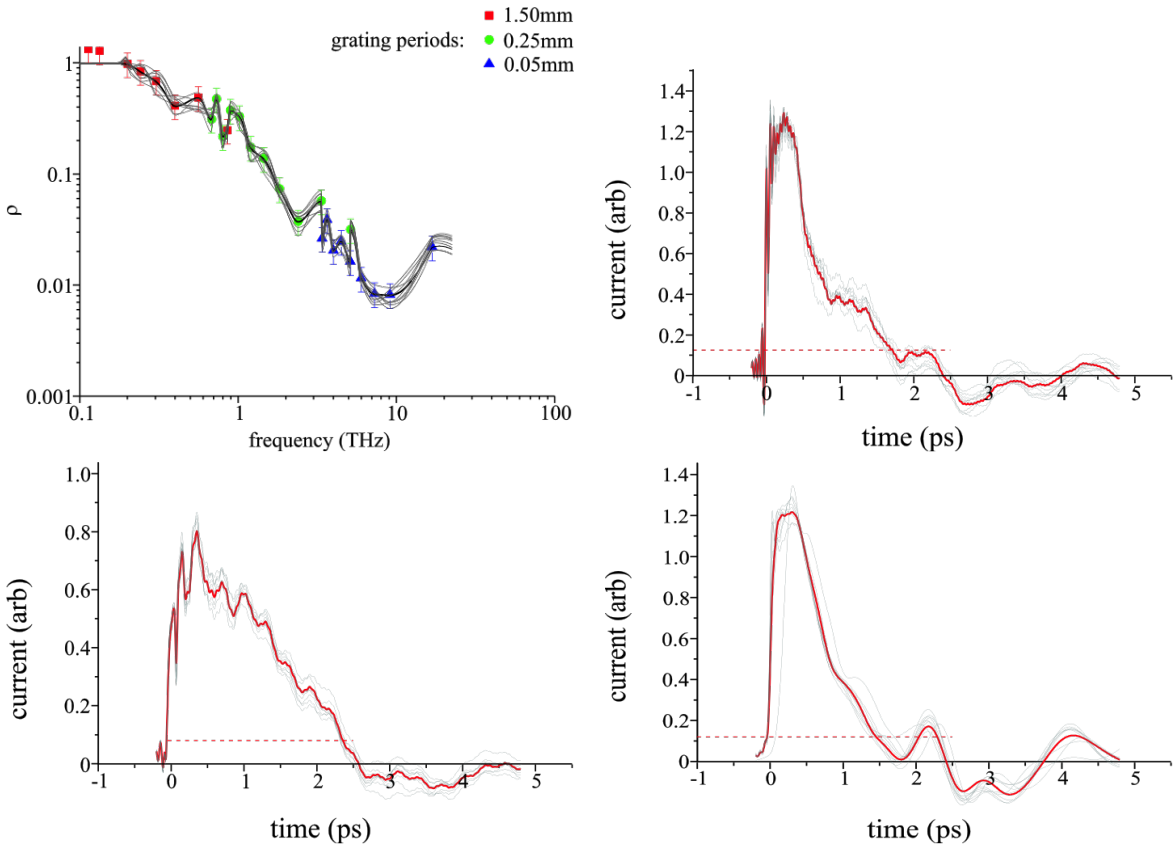

Figure 1.21: Top left: The magnitude of the Fourrier Transform of the time profile of the bunch for a ?high compression? run on the 9 April 2013 (see text in [42]). Other plots: bunch profile reconstructed from measurements at different times and with different bunch compression settings (top right: 9 April 2013, high compression; bottom left: 9 April 2013, medium compression; bottom right: 25 june 2013). Plots taken from [42] where more explanations can be found.

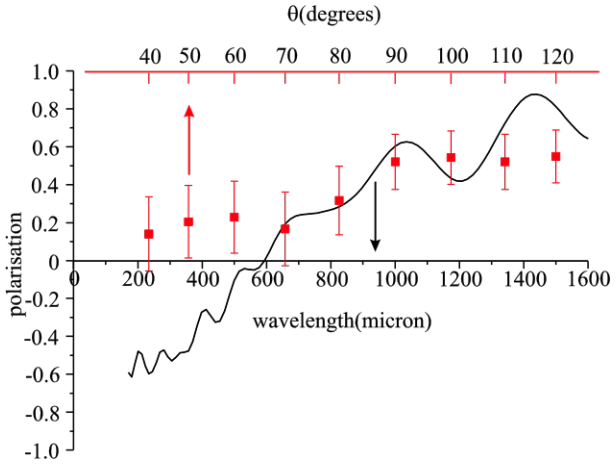

Figure 1.22: The measured degree of polarisation of the grating signal as a function of observation angle. The solid line is the theoretically predicted polarisation of CSPR, as a function of wavelength (see text in [42] for details; plot taken from [42]).

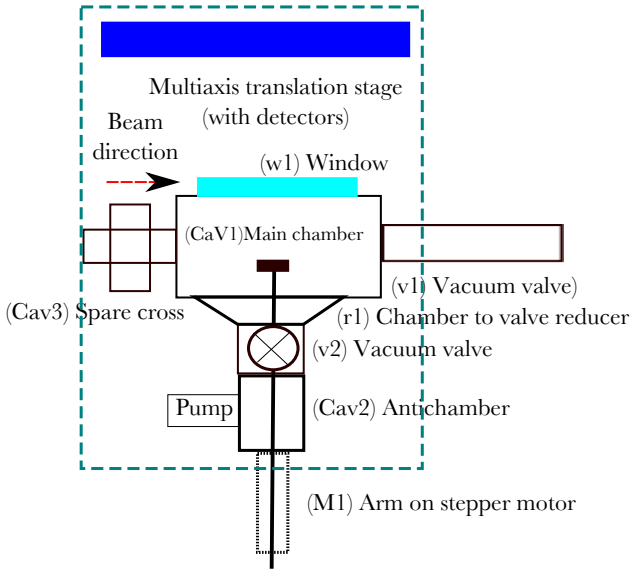

Figure 1.23: The experimental setup of SPESO at the end of the SOLEIL Linac (image taken from [57]).

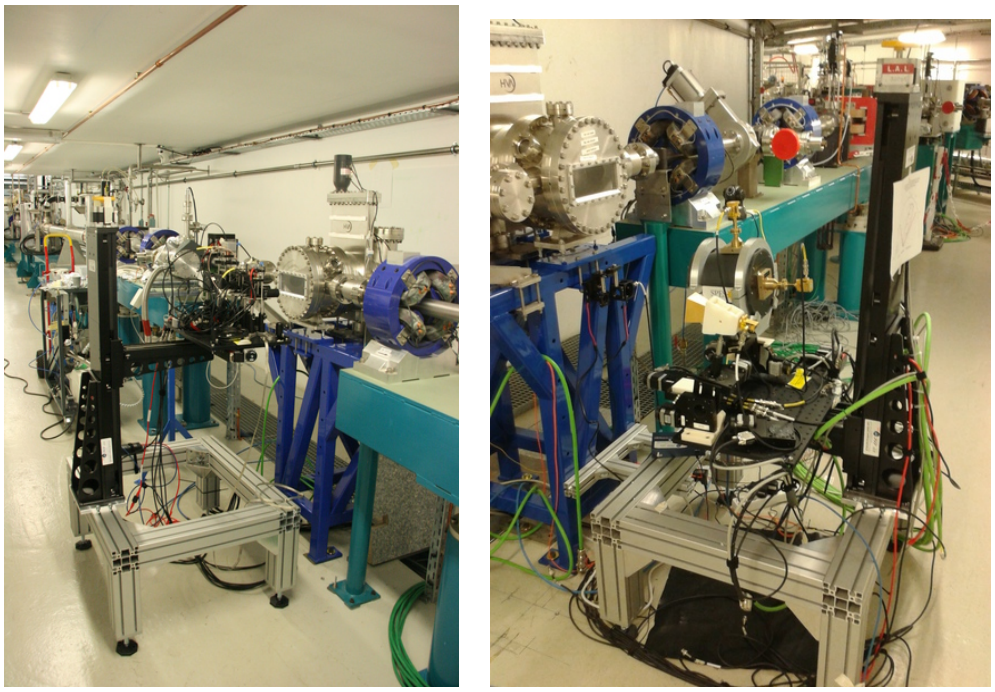

Figure 1.24: The experimental setup of SPESO at the end of the SOLEIL Linac: left, as it was in 2015 (image taken from [57]) and right with the polarizer installed in 2016 (image taken from [58]). On both images the electrons travels from left to right.

derestimated. After some searching we finally found some signal at wavelength much longer than expected (see figure 1.25). These data allowed us to reconstruct the spectrum emitted by the bunch and its profile (see figure 1.26). These results were reported in [59] where detailed explanations of these figures are available. Discussion with persons who contributed to the commissioning of the linac showed that our measurement is in agreement with the measurements done during the linac commissioning.

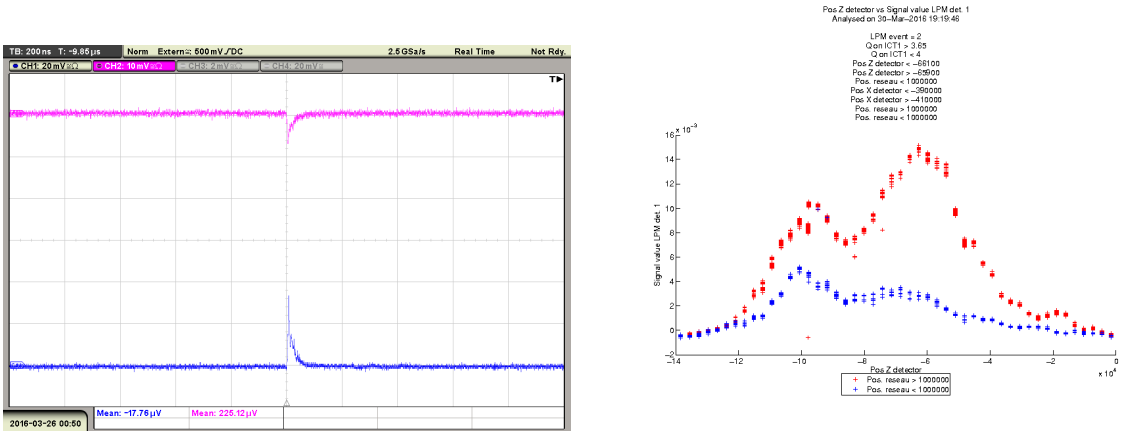

Figure 1.25: Left: Example adapted from [59] of the initial data recorded with the two SPESO detectors (Pink is the Q-band detector and blue is the Ka-band detector, see explanation in [59]). Right: Example taken from [59] of raw signal collected with the the Ka-band detector while the detectors were moving vertically. The red line corresponds to the grating in the inserted position and the blue line to the grating in the retracted position (background).

The SPESO experiment has been upgraded in 2016 to study the polarisation of the Smith-Purcell radiation. The result has been presented in [58] and is shown in figure 1.27. This result is a surprise to us as we expected almost 100% polarization but it could be compatible with what was observed at FACET (see figure 1.22). The measurement campaign on SPESO is continuing to increase the range of the measurement.

1.3.3 Coherent Smith-Purcell radiation measurement at CLIO.

SPESO is meant to be a test bench to study the properties of Coherent Smith-Purcell Radiation. However to have this diagnostic accepted in control rooms, it is necessary to demonstrate that it can work as a control room tool and produce results quickly. This is the aim of the Smith-Purcell experiment at CLIO. CLIO (Acronym in french for Infrared Laser Center at Orsay - *Centre Laser Infrarouge à Orsay*) is a Free Electron Laser installed in Orsay. It has been described in [60, 61, 62].

Before installing the experiment we studied the dynamics of the beam and the predicted signal [45]. Example of expected signal are shown on figure 1.28. To avoid searching the

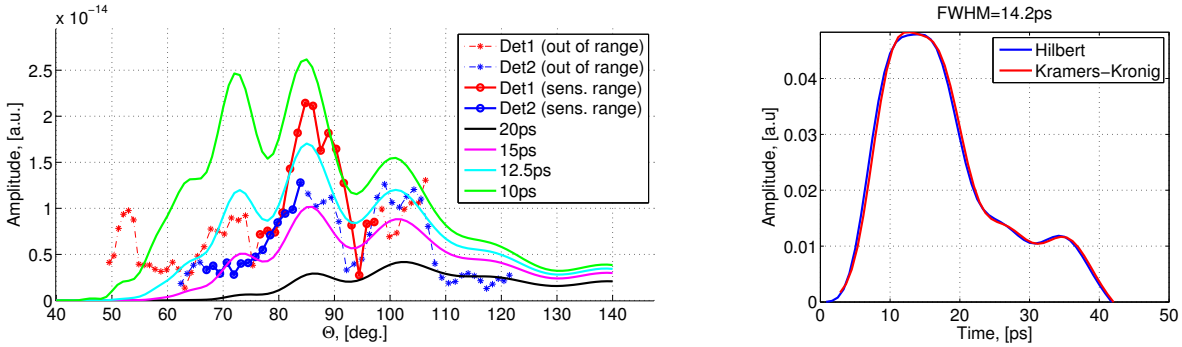

Figure 1.26: Images taken from [59]. Left: Distribution of the signal measured as function of the observation angle. The red dots correspond to the Ka band detector and the blue dots to the Q-band detector. The solid lines correspond to data points at frequencies within the sensitivity range of the detector and the dashed lines to data points at frequencies outside that range. These data are compared to simulations for 4 different bunch FWHM. Right: Bunch profile recovered from the data presented on the left using the method described in [53].

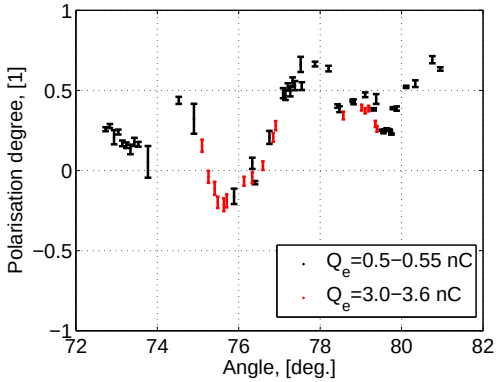

Figure 1.27: Degree of polarisation as function of the longitudinal displacement (along the beam propagation axis). Image taken from [58].

signal for too long in case the pulse length was very different from the expectations we decided to first measure CTR and made a comparison of expected signal level for CTR and CSPR [63]. On figure 1.29 the single electron yield and the predicted spectrum at CLIO are compared. Our conclusion was that using the CLIO parameters and with a beam-grating separation of 3 mm we expect a signal (in the range 0.03-3 THz [0.1 - 10 mm]) of 8.37×10^{-7} J for CSPR and 7.35×10^{-8} J for CTR. This result was questioned by a few colleagues but finally accepted and confirmed by independent experimental verifications made at another facility by another group [64].

After a first phase during which we measured CTR to validate the detection chain the

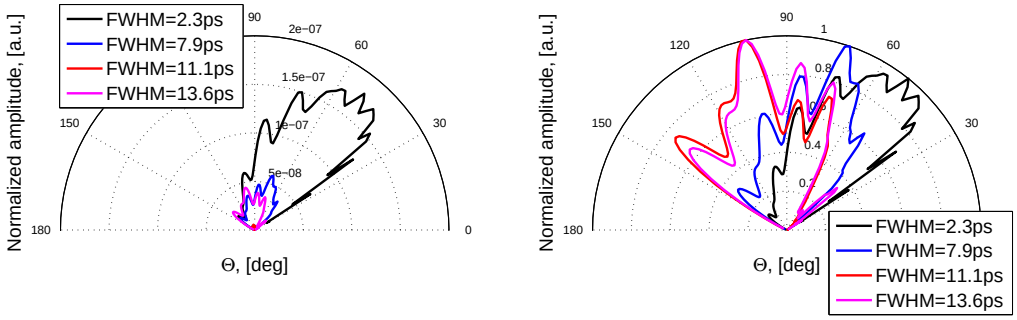

Figure 1.28: Coherent Smith-Purcell spectrum as a function of the observation angle for different bunch profiles in CLIO. The grating used for these simulations has a pitch of 8 mm and a blaze angle of 30^o. The left figure gives the energy distribution, the right figure is normalized so that the maximum amplitude of each line is 1. Image taken from [45].

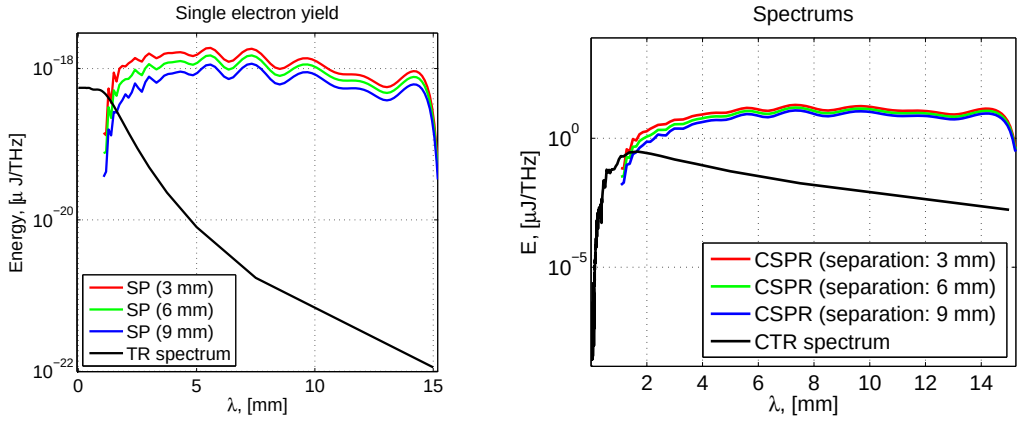

Figure 1.29: Left: Single electron yield for transition radiation (TR) and Smith-Purcell radiation (SP). The screen diameter for transition radiation is 40 mm. The SP single electron yield is presented for different beam-grating separation (3 mm, 6 mm and 9 mm). The grating used here is 40×180 mm^2 with 8 mm pitch and 30^o blaze angle. The signal is measured as integrated with a 50 mm diameter parabolic mirror located 300 mm from the beam axis. Right: CSPR and CTR energy density as function of wavelength with the same parameters than on the left figure. Both images are taken from [45].

experiment has quickly been upgraded with a grating instead of the CTR screen. Unlike the E-203 experiment we use single quartz window to let the radiation out. We also decided to use Off Axis Parabolic mirrors (OAP) instead of Winston cones to focus the radiation of the detectors. Photos of the experiment are shown on figure 1.30 and the

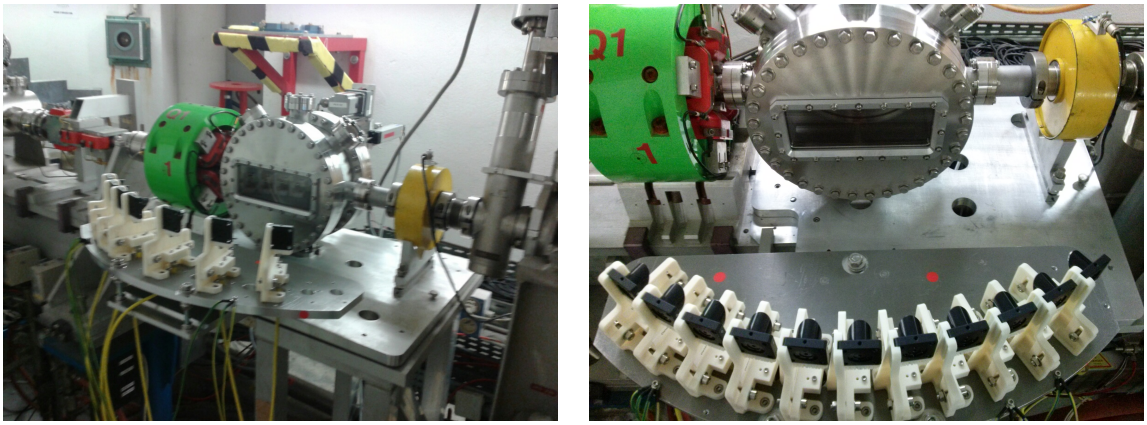

Figure 1.30: The experimental setup for CSPR measurements at CLIO: a set of pyrodectors with off axis parabolic mirrors is placed equidistantly with 7° separation around the window and the experimental chamber with the grating inside (right image taken from [65]). The two images have been taken at different dates and have a different number of detectors.

experiment has been described in details in [65].

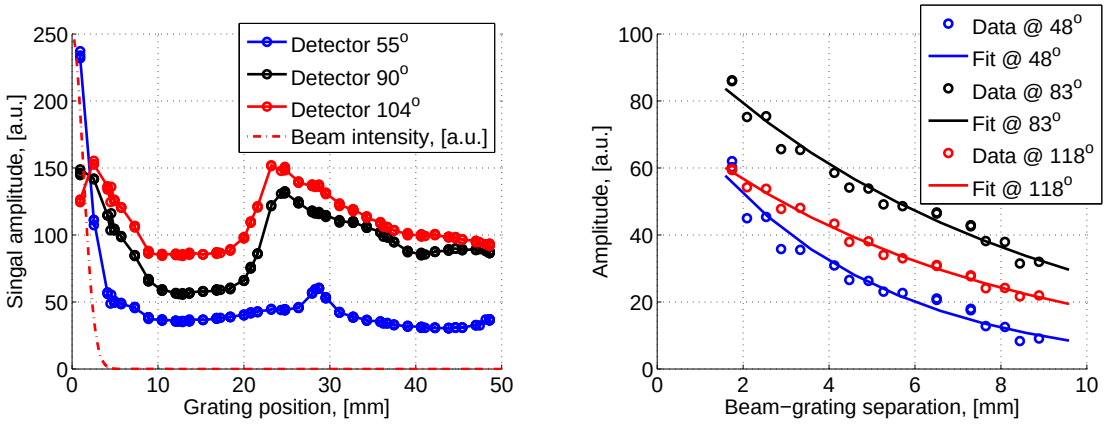

Figure 1.31: Signal amplitude as function of the grating position with respect to the center of the beam for three different detectors angles for a long range (left) and a short range near the beam (right). On the right the data (circles) is compared to a fit (solid line). Images taken form [65]. On the left image the peak between 20 mm and 30 mm is still under investigations.

After the publication of [65] further work was done and has been reported in [66]. The figure 1.32 shows form factors that were measured on CLIO and figure 1.33 shows the reconstructed profile.

During the recent runs we took data with two different grating pitches. As the data

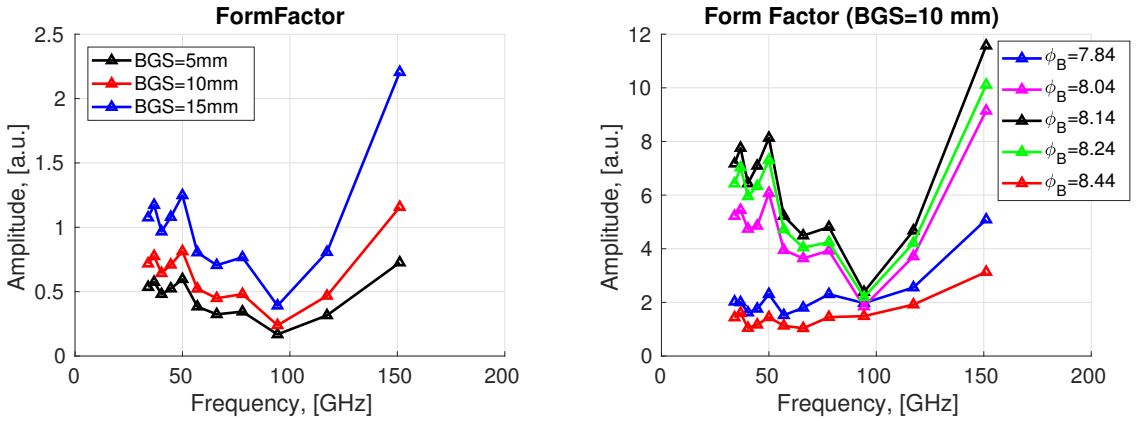

Figure 1.32: Form factor measured at CLIO as reported in [66]. Left: Variation of the form factor when the beam grating separation varies. Right: Variation of the form factor when the buncher phase varies.

were taken on different days (at the moment changing the grating requires breaking the vacuum) it is difficult to put them together but the comparisons we did look promising.

The experiment will be upgraded in a few months so that we will be able to change the grating without breaking the vacuum. We also hope to be able to test strategies were 3 gratings will be exposed at the same time (at different azimuthal angles) to be able to do single shot measurements a scheme showing a transverse view of such layout is shown on figure 1.34.

1.3.4 Outlook: Application to laser-driven plasma accelerators, ERLs and the ESS

Coherent Smith-Purcell Radiation has the potential to become a single shot diagnostic to measure longitudinal profile.

One of the initial motivation for this diagnostic is to be able to measure the longitudinal profile of beams coming out of plasma accelerators. The very short pulses produced by such accelerator make them a very interesting topic to study and the ESCULAP facility at LAL (see section 1.4) will offer good testing opportunities. One important question that CSPR should allow to settle on a plasma acceleration experiment is wether the electron pulse has been produced alone or if it accompanied by satellites in the neighboring buckets.

However on the way other applications have appeared. The European Spallation Facility will have ps-bunches in its high energy and their length will have to be measured non destructively. CSPR is well suited for such measure as it is non intercepting and some

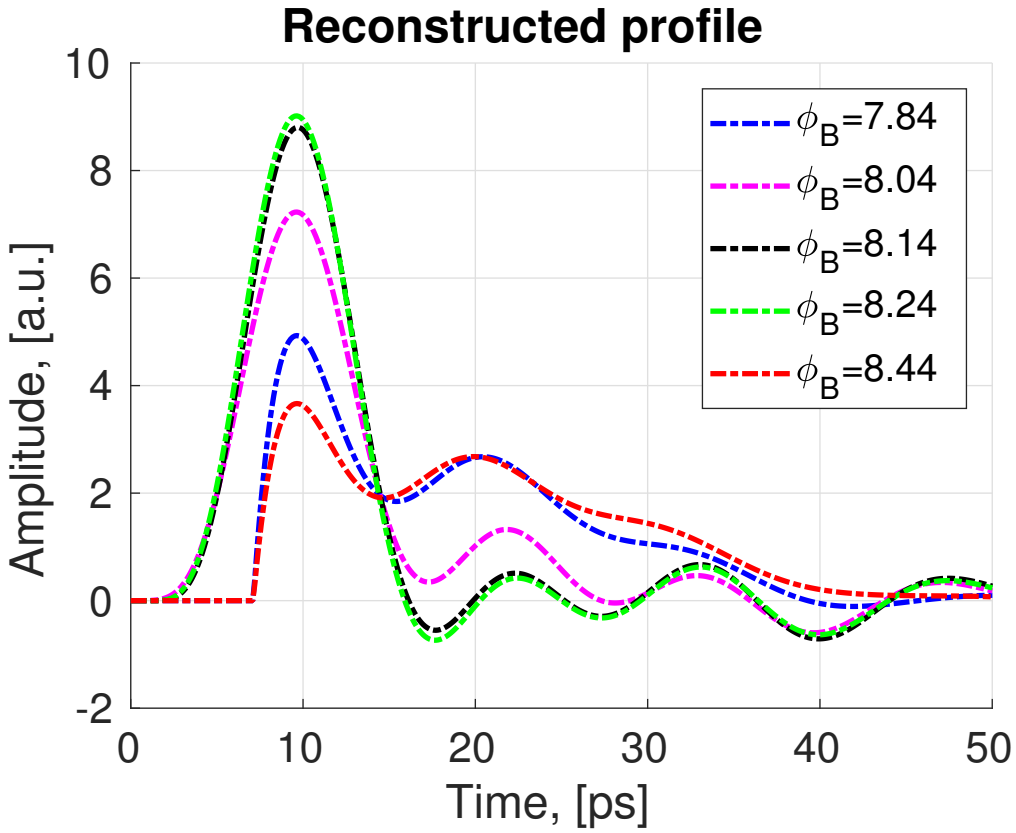

Figure 1.33: Bunche profile reconstructed on CLIO for different buncher phase as reported in [66].

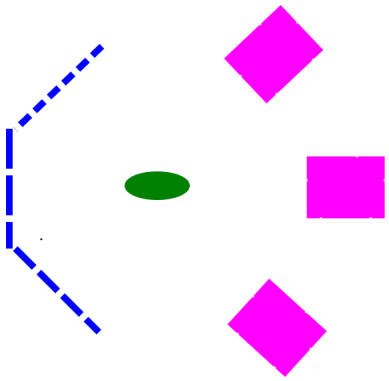

Figure 1.34: Proposed scheme for single show measurement: in the transverse plane three different grating, 60° apart are used to measure three different wavelength ranges from the beam.

preliminary studies have been performed [**?**]. Another location where the non intercepting nature of CSPR combined to the moderate cost of the associated detector can be an advantage is Energy Recovery Linacs (ERL). In an ERL longitudinal deformation of the electron bunch can be amplified at each pass leading to beam disruption. A monitor capable of monitoring the bunch profile at several locations without destroying it is therefore important. This can be done by a CSPR monitor.

1.4 Undefined references

chap:plasmaAccelerationMecanism chap:laser-wire chap:pepper-pot chap:SP laser-synch chap:laser-plasma sec:ESCULAP sec:OTR interference

Bibliography

[1] M. Litos, E. Adli, W. An, C. I. Clarke, C. E. Clayton, S. Corde, J. P. Delahaye, R. J. England, A. S. Fisher, J. Frederico, S. Gessner, S. Z. Green, M. J. Hogan, C. Joshi, W. Lu, K. A. Marsh, W. B. Mori, P. Muggli, N. Vafaei-Najafabadi, D. Walz, G. White, Z. Wu, V. Yakimenko, and G. Yocky. High-efficiency acceleration of an electron beam in a plasma wakefield accelerator. *Nature*, 515(7525):92–95, 11 2014.

[2] Allen Caldwell, Konstantin Lotov, Alexander Pukhov, and Frank Simon. Proton-driven plasma-wakefield acceleration. *Nat Phys*, 5(5):363–367, 05 2009.

[3] Nicolas Delerue, Christelle Bruni, Stéphane Jenzer, Sophie Kazamias, Bruno Lucas, Gilles Maynard, and Moana Pittman. Simulations of the Acceleration of Externally Injected Electrons in a Plasma Excited in the Linear Regime. In *arXiv 1607.02065 - IPAC'16, WEPMY0003*, 2016.

[4] Bergoz http://www.bergoz.com/ict-bcm-ihr.

[5] G. Devanz, B. Leblond, B. Mouton, and C. Travier. Bunch length measurement on CANDELA photoinjector. *Conf. Proc.*, C9608262:761–763, 1996.

[6] C. M. Thomas and G. Rehm. Diamond optical diagnostics: First streak camera measurements. *Conf. Proc.*, C060626:1112–1114, 2006. [,1112(2006)].

[7] M.-E. Couprie R. Nagaoka D. Pedeau M. Labat, L. Cassinari. Streak camera measurements of the soleil bunch length. In *Proceedings, DIPAC 2007*, page wepb05, 2007.

[8] Valery A. Dolgashev, Gordon Bowden, Yuantao Ding, Paul Emma, Patrick Krejcik, James Lewandowski, Cecile Limborg, Michael Litos, Juwen Wang, and Dao Xiang. Design and application of multimegawatt x-band deflectors for femtosecond electron beam diagnostics. *Phys. Rev. ST Accel. Beams*, 17:102801, Oct 2014.

[9] F. Glotin, J.-M. Berset, R. Chaput, D. A. Jaroszynski, J.-M. Ortéga, and R. Prazérès. Bunch length measurements on CLIO. *Nuclear Instruments and Methods in Physics Research A*, 341:49–53, March 1994.

[10] Thomas Vinatier, Christelle Bruni, Sophie Chancé, and Patrick Puzo. Length Measurement of High-brightness Electron Beam thanks to the 3-Phase Method. In *Proceedings, 5th International Particle Accelerator Conference (IPAC 2014): Dresden, Germany, June 15-20, 2014*, page THPME095, 2014.

[11] X. Yan, A. M. MacLeod, W. A. Gillespie, G. M. H. Knippels, D. Oepts, A. F. G. van der Meer, and W. Seidel. Subpicosecond electro-optic measurement of relativistic electron pulses. *Phys. Rev. Lett.*, 85:3404–3407, Oct 2000.

[12] Y Parc, Changbum Kim, Jung Yun Huang, Jangho Park, Taiha Joo, and In Soo Ko. A study of electro-optical crystal as a diagnostic tool for low energy electron beam. *JOURNAL-KOREAN PHYSICAL SOCIETY*, 50(5):1390, 2007.

[13] H. Tomizawa, T. Sato, K. Ogawa, K. Togawa, T. Tanaka, T. Hara, M. Yabashi, H. Tanaka, T. Ishikawa, T. Togashi, and et al. Stabilization of a high-order harmonic generation seeded extreme ultraviolet free electron laser by time-synchronization control with electro-optic sampling. *High Power Laser Science and Engineering*, 3, 2015.

[14] T. J Maxwell, C. Beherens, Y. Ding, A. S. Fisher, J. Frisch, Z. Huang, and H. Loos. Coherent Radiation Spectroscopy of Few-Femtosecond Electron Bunches Using a Middle-Infrared Prism Spectrometer. *Phys. Rev. Lett.*, 111(18):184801, 2013.

[15] E. Chiadroni, M. Bellaveglia, P. Calvani, M. Castellano, L. Catani, A. Cianchi, G. Di Pirro, M. Ferrario, G. Gatti, O. Limaj, S. Lupi, B. Marchetti, A. Mostacci, E. Pace, L. Palumbo, C. Ronsivalle, R. Pompili, and C. Vaccarezza. Characterization of the thz radiation source at the frascati linear accelerator. *Review of Scientific Instruments*, 84(2):022703, 2013.

[16] Stephan Wesch, Bernhard Schmidt, Christopher Behrens, Hossein Delsim-Hashemi, and Peter Schmuser. A Multi-Channel THz and Infrared Spectrometer for Femtosecond Electron Bunch Diagnostics by Single-Shot Spectroscopy of Coherent Radiation. *Nucl. Instrum. Meth.*, A665:40–47, 2011.

[17] M. D. Litos, M. R. Bionta, V. A. Dolgashev, R. J. England, D. Fritz, S. Gilevich, Ph. Hering, and M. J. Hogan. Evaluation of Temporal Diagnostic Techniques for Two-Bunch FACET Beam. *Conf. Proc.*, C110328:568–570, 2011.

[18] S. J. Smith and E. M. Purcell. Visible light from localized surface charges moving across a grating. *Phys. Rev.*, 92:1069–1069, Nov 1953.

[19] G. Doucas, J. H. Mulvey, M. Omori, J. Walsh, and M. F. Kimmitt. First observation of smith-purcell radiation from relativistic electrons. *Phys. Rev. Lett.*, 69:1761–1764, Sep 1992.

[20] K. Ishi, Y. Shibata, T. Takahashi, S. Hasebe, M. Ikezawa, K. Takami, T. Matsuyama, K. Kobayashi, and Y. Fujita. Observation of coherent smith-purcell radiation from short-bunched electrons. *Phys. Rev. E*, 51:R5212–R5215, Jun 1995.

[21] K. Ishiguro and T. Tako. An Estimation of Smith-Purcell Effect as the Light Source in the Infra-red Region. *Optica Acta*, 8:25–31, 1961.

[22] G. Toraldo di Francia. On the theory of some Čerenkovian effects. *Il Nuovo Cimento*, 16:61–77, April 1960.

[23] D. V. Karlovets and A. P. Potylitsyn. Comparison of smith-purcell radiation models and criteria for their verification. *Phys. Rev. ST Accel. Beams*, 9:080701, Aug 2006.

[24] M.S. Malovytsia and N. Delerue. Comparison of the Smith-purcell Radiation Yield for Different Models . In *IPAC2016*, Proceedings of IPAC2016, page MOPMB004, Busan, South Korea, May 2016.

[25] D.V. Karlovets and A.P. Potylitsyn. Smith-purcell radiation in the ?pre-wave? zone. *JETP Letters*, 84(9):489–493, 2007.

[26] J. H. Brownell, J. Walsh, and G. Doucas. Spontaneous Smith-Purcell radiation described through induced surface currents. *Phys. Rev. E*, 57:1075–1080, Jan 1998.

[27] C.A. Ekdahl. High power microwave generator, June 24 1986. US Patent 4,596,967.

[28] J. M. Wachtel. Free-electron lasers using the smith-purcell effect. *Journal of Applied Physics*, 50(1):49–56, 1979.

[29] Levi Schächter and Amiram Ron. Smith-purcell free-electron laser. *Phys. Rev. A*, 40:876–896, Jul 1989.

[30] H. L. Andrews and C. A. Brau. Gain of a smith-purcell free-electron laser. *Phys. Rev. ST Accel. Beams*, 7:070701, Jul 2004.

[31] J. Gardelle, P. Modin, and J. T. Donohue. Start current and gain measurements for a smith-purcell free-electron laser. *Phys. Rev. Lett.*, 105:224801, Nov 2010.

[32] P Rullhusen, X Artru, and P Dhez. *Novel radiation sources using relativistic electrons: from infrared to x-rays*. Synchrotr Radiat. Techniques Appl. World Scientific, Singapore, 1998.

[33] C. Brau, C. Boulware, and H. Andrews. Smith-purcell free electron laser and method of operating same, March 23 2006. US Patent App. 11/172,429.

[34] D.C. Nguyen. Measuring short electron bunch lengths using coherent smith-purcell radiation, March 30 1999. US Patent 5,889,797.

[35] A. Doria, G.P. Gallerano, E. Giovenale, G. Messina, G. Doucas, M.F. Kimmitt, H.L. Andrews, and J.H. Brownell. Can coherent smith–purcell radiation be used to determine the shape of an electron bunch? *Nuclear Instruments and Methods in Physics Research Section A: Accelerators, Spectrometers, Detectors and Associated Equipment*, 483(1):263 – 267, 2002. Proceedings of the 23rd International Free Electron Laser Confere nce and 8th FEL Users Workshop.

[36] G. Doucas, M. F. Kimmitt, A. Doria, G. P. Gallerano, E. Giovenale, G. Messina, H. L. Andrews, and J. H. Brownell. Determination of longitudinal bunch shape by means of coherent smith-purcell radiation. *Phys. Rev. ST Accel. Beams*, 5:072802, Jul 2002.

[37] G. Doucas et al. Longitudinal electron bunch profile diagnostics at 45-MeV using coherent Smith-Purcell radiation. *Phys. Rev. ST Accel. Beams*, 9:092801, 2006.

[38] V. et al. Blackmore. First measurements of the longitudinal bunch profile of a 28.5 GeV beam using coherent Smith-Purcell radiation. *Phys. Rev. ST Accel. Beams*, 12:032803, Mar 2009.

[39] Nicolas Delerue, George Doucas, Ewen Maclean, and Armin Reichold. Longitudinal bunch profile diagnostics in the 50fs range using coherent Smith-Purcell radiation. 2009.

[40] R Bartolini, C Clarke, N Delerue, G Doucas, and A Reichold. Electron bunch profile reconstruction in the few fs regime using coherent Smith-Purcell radiation. *Journal of Instrumentation*, 7(01):P01009, 2012.

[41] H.L. Andrews, F. Bakkali Taheri, J. Barros, R. Bartolini, L. Cassinari, C. Clarke, S. Le Corre, N. Delerue, G. Doucas, N. Fuster-Martinez, I. Konoplev, M. Labat, C. Perry, A. Reichold, S. Stevenson, and M. Vieille Grosjean. Longitudinal profile monitors using coherent Smith-Purcell radiation. In Jens Osterhoff Arnd E. Specka Ralph Assmann, Massimo Ferrario, editor, *1st European Advanced Accelerator Concepts Workshop (EAAC2013)*, volume 740, pages 212–215, La Biodola, Italy, June 2013. Elsevier.

[42] L. Andrews, H. F. Bakkali Taheri, J. Barros, R. Bartolini, V. Bharadwaj, C. Clarke, N. Delerue, G. Doucas, N. Fuster-Martinez, M. Vieille-Grosjean, V. Konoplev, I. M. Labat, S. Le Corre, C. Perry, A. Reichold, and S. Stevenson. Reconstruction of the time profile of 20.35 gev, subpicosecond long electron bunches by means of coherent smith-purcell radiation. *Phys. Rev. ST Accel. Beams*, 17:052802, May 2014.

[43] J H Brownell, G Doucas, M F Kimmitt, J H Mulvey, M Omori, and J E Walsh. The angular distribution of the power produced by smith-purcell radiation. *Journal of Physics D: Applied Physics*, 30(17):2478, 1997.

[44] http://www.tau.ac.il/ phchlab/. Spectrum of the hydrogen atom.

[45] N. Delerue, S. Jenzer, V. Khodnevych, J-P. Berthet, F. Glotin, J-M. Ortega, and R. Prazeres. Study of Short Bunches at the Free Electron Laser CLIO. In *IPAC2016*, Proceedings of IPAC2016, page MOPMB005, Busan, South Korea, May 2016.

[46] J. H. Brownell and G. Doucas. Role of the grating profile in Smith-Purcell radiation at high energies. *Phys. Rev. ST Accel. Beams*, 8:091301, 2005.

[47] C. A. J. Palmer and Loewen E. *Diffraction grating handbook*. Newport Corporation, 2005.

[48] Solène Le Corre. Study of the polarization of smith-purcell radiation. Master's thesis, ENS Lyon, 2012.

[49] D.A. Zhuravlev. E. g. loewen and e. popov diffraction gratings and their applications (marcel dekker, new york, 1997). *Optics and Spectroscopy*, 88(1):143–144, 2000.

[50] F. Bakkali Taheri, G. Doucas, I.V. Konoplev, A. Reichold, S.R. Stevenson, H.I. Andrews, R. Bartolini, V. Bharadwaj, C.I. Clarke, N. Delerue, N. Fuster Martinez, D.A. Smith, and P. Stoltz. Spectra of Coherent Smith-Purcell Radiation Observed from Short Electron Bunches: Numerical and Experimental Studies. In *IPAC 13 - 4th International Particle Accelerator Conference*, pages 801–803, Shanghai, China, May 2013. Joint Accelerator Conferences Website. MOPWA056 - ISBN978-3-95450-122-9.

[51] O. Grimm and P. Schmüser. Principles of longitudinal beam diagnostics with coherent radiation. *TESLA FEL note*, page 03, 2006.

[52] N. Delerue, J. Barros, M. Vieille-Grosjean, O. Bezshyyko, V. Khodnevych, and T. Shevchenko. Study of phase reconstruction techniques applied to Smith-Purcell radiation measurements. 5th International Particle Accelerator Conference IPAC'14, June 2014. Poster - Work supported by the French ANR (contract ANR-12-JS05-0003-01), the PICS (CNRS) "Development of the instrumentation for accelerator experiments, beam monitoring and other applications and Research Grant F58/380-2013 - (project F58/04) from the State Fund for Fundamental Researches of Ukraine in the frame of the State key laboratory of high energy physics." - http://accelconf.web.cern.ch/AccelConf/IPAC2014/papers/thpme088.pdf.

[53] Nicolas Delerue, Joanna Barros, Oleg Bezshyyko, and Vitalii Khodnevych. Study of Phase Reconstruction Techniques applied to Smith-Purcell Radiation Measurements. *ArXiV*, 2015.

[54] Maksym Malovystia. Simulation of the smith-purcell radiation and designing stepper motor control system. Technical report, LIA IDEATE France-Ukraine, 2015.

[55] C Thomas, N Delerue, and R Bartolini. Single shot transverse emittance measurement from otr screens in a drift transport section. *Journal of Instrumentation*, 6(07):P07004, 2011.

[56] J. Amann et al. Facility for Advanced Accelerator Experimental Tests at SLAC (FACET) Conceptual Design Report. 2009.

[57] N. Delerue, J. Barros, S. Jenzer, M. Vieille Grosjean, L. Cassinari, M. Labat, G. Doucas, I.V. Konoplev, A. Reichold, A. Faus-Golfe, N. Fuster Martinez, and J. Resta-Lopez. Presentation of the Smith-Purcell Experiment at SOLEIL. IBIC2013 - 2nd International Beam Instrumentation Conference, September 2013.

Poster - TUPC37 - Work supported by seed funding from Université Paris-Sud, program "Attractivité" and by the ANR under contract ANR-12-JS05-0003-01.

[58] Nicolas Delerue, Joanna Barros, Nicolas Hubert, Stéphane Jenzer, Vitalii Khodnevych, Marie Labat, and Maksym Malovytsia. Ipac 17 soleil. page MOPMB002, 2017.

[59] Nicolas Delerue, Joanna Barros, Nicolas Hubert, Stéphane Jenzer, Vitalii Khodnevych, Marie Labat, and Maksym Malovytsia. First Measurements of Coherent Smith-Purcell Radiation in the SOLEIL Linac. In *Proceedings, 7th International Particle Accelerator Conference (IPAC 2016): Busan, Korea, May 8-13, 2016*, page MOPMB002, 2016.

[60] M. Ageron et al. Study report on free electron laser project with 3-GHz HF Linear Accelerator (Collaboration For An Infrared Laser at Orsay). *LAL-RT-89-04*, 1989.

[61] J.C. Bourdon, R. Belbeoch, M. C. Bernard, P. Brunet, B. Leblond, M. Omeich, E. Plouviez, J. Rodier, R. Chaput, M. Bergher, and J.M. Ortega. Commissioning the Clio injection system. In *Free Electron Laser International Conference 12*, volume 304, pages 322–328, Paris, France, September 1990. Elsevier.

[62] F. Glotin et al. First lasing of the CLIO FEL. *Conf. Proc.*, C920324:620–622, 1992.

[63] N. Delerue, V. Khodnevych, and O. Bezshyyko. Comparison of Coherent Smith-Purcell Radiation and Coherent Transition Radiation. In *IPAC2016*, Proceedings of IPAC2016, page MOPMB003, Busan, South Korea, May 2016.

[64] A. Aryshev, A. Potylitsyn, G. Naumenko, M. Shevelev, K. Lekomtsev, L. Sukhikh, P. Karataev, Y. Honda, N. Terunuma, and J. Urakawa. Monochromaticity of coherent smith-purcell radiation from finite size grating. *Phys. Rev. Accel. Beams*, 20:024701, Feb 2017.

[65] Nicolas Delerue and Vitalii Khodnevych. Ipac 17 clio. 2017.

[66] Vitalii Hodnevych. Clio report. Master's thesis, Unpublished, 2017.